

Methods of Fourier–Stokes polarimetry and the spatial-frequency filtering in the diagnostic tasks

A.G. Ushenko¹, A.V. Dubolazov¹, M.Yu. Sakhnovskiy¹, A.V. Motrich¹, Yu.A.Ushenko¹, L.Y. Pidkamin¹, L.Ya. Kushnerik¹, M.S. Gavrylyak¹, P. Grygorishin²

¹Chernivtsi National University,

2, Kotsyubinsky str., 58012 Chernivtsi, Ukraine

²Bukovinian State Medical University,

58000 Chernivtsi, Ukraine,

e-mail: o.dubolazov@chnu.edu.ua

Abstract. The optical model of polycrystalline networks in human skin has been suggested. The results of investigation of the values of statistical (statistical moments of the 1st to 4th orders) parameters describing polarization of inhomogeneous images obtained for skin surface in Fourier domain have been presented. The diagnostic criteria of pathological processes in human skin and its severity degree differentiation have been determined.

Keywords: polarization, Fourier optics and signal processing, imaging systems, medical and biological imaging, polarization speckle.

Manuscript received 11.11.16; revised version received 25.01.17; accepted for publication 01.03.17; published online 05.04.17.

1. Introduction

Investigations *in vitro* prevail among various optical and physical techniques for diagnosing the structure and properties of biological objects [1-11]. Particularly, laser polarimetry of microscopic images inherent to polycrystalline protein networks was formed as a separate approach for studying optically anisotropic components in histological sections of different biological tissues biopsy [12-19]. The analytical methods used in laser polarimetry are based on approximation of linear birefringence in biological tissues. On the base of the above mentioned approach, it has been found the interrelation between the set of statistic moments of the 1st to 4th orders, which characterize the azimuth and ellipticity distributions of laser images, and the physiological state of biological tissue layer. As a result, the method of polarization mapping and the successful diagnostics of oncological

(malignant) changes in human biological tissues have been elaborated.

2. Basic analytical relations

In order to extend the functional possibilities of oncological diagnostics, application of polarization mapping the biological tissues *in vivo* is topical. In this situation, obtaining the convenient microscopic images is complicated, which is caused by a high level of diffuse background. Fourier polarimetry of biological tissue can be used as an alternative approach [20]. This method allows to concentrate radiation reflected from biological tissue and to perform polarization mapping the obtained polarization inhomogeneous field in the Fourier plane. At the same time, polarization structure of these object fields of biological tissues *in vivo* remains practically unstudied. This research is aimed at investigation of efficiency of optical differentiation of benign (adenoma) and pre-cancer (keratoma) changes of

human skin by using the statistical analysis of polarization inhomogeneous scattered laser radiation in the Fourier plane.

In [12, 16-18], it was proposed and experimentally proved the model of amorphous-crystalline structure of planar layers in the main types of biological tissues – connective, muscular, epithelial and nervous. Within the limits of this approach, it has been shown that the following matrix operator can characterize the optical manifestations of polycrystalline networks anisotropy [20]

$$P = \begin{vmatrix} p_{11}(\rho, \gamma, \psi) & p_{12}(\rho, \gamma, \psi) \\ p_{21}(\rho, \gamma, \psi) & p_{22}(\rho, \gamma, \psi) \end{vmatrix} = \begin{vmatrix} (\sin^2 \rho + \cos^2 \rho \exp(-i\omega)) & (\cos^2 \rho + \sin^2 \rho \exp(-i\omega)) \\ (\cos^2 \rho + \sin^2 \rho \exp(-i\omega)) & (\sin^2 \rho + \cos^2 \rho \exp(-i\omega)) \end{vmatrix} \times \begin{vmatrix} \cos \psi & \sin \psi \\ -\sin \psi & \cos \psi \end{vmatrix} \quad (1)$$

where $p_{ik}(\rho, \gamma, \psi)$ are the Jones-matrix elements defined by directions of optical axes ρ in biological crystals and the values of phase shifts for linear (γ) and circular (ψ) birefringence.

In accordance with (1), the processes of formation of laser field in the polycrystalline network in the plane of biological layer is quite completely described by the following Jones-matrix equation

$$\begin{pmatrix} U_x e^{i\gamma_x} \\ U_y e^{i\gamma_y} \end{pmatrix} = \begin{vmatrix} p_{11} & p_{12} \\ p_{21} & p_{22} \end{vmatrix} \begin{pmatrix} U_{0x} e^{i\gamma_{0x}} \\ U_{0y} e^{i\gamma_{0y}} \end{pmatrix} = \begin{pmatrix} p_{11} U_{0x} e^{i\gamma_{0x}} + p_{12} U_{0y} e^{i\gamma_{0y}} \\ p_{21} U_{0x} e^{i\gamma_{0x}} + p_{22} U_{0y} e^{i\gamma_{0y}} \end{pmatrix} \quad (2)$$

Here, γ_{0x}, γ_{0y} are the phases of orthogonal components (U_{0x}, U_{0y}) of the amplitude of laser beam probing the polycrystalline network, γ_x, γ_y – phases of orthogonal components U_x, U_y of the laser field amplitude in the plane of biological layer.

From the equation (2), it is possible to determine the trajectory of polarization waves in every point (x, y) of the laser image

$$\frac{x^2}{U_x^2} - \frac{2xy}{U_x U_y} \cos \Delta\gamma + \frac{y^2}{U_y^2} = \sin^2 \Delta\gamma. \quad (3)$$

Here, $\Delta\gamma = \gamma_x - \gamma_y$.

Thus, polarization inhomogeneous (polarization maps $\alpha(x, y), \beta(x, y)$) image of biological tissue layer is formed [18]

$$\alpha(x, y) = 0.5 \arcsin \left[\frac{\sin 2\Theta(x, y)}{\cos \Delta\gamma(x, y)} \right], \quad (4)$$

$$\beta(x, y) = 0.5 \arctan \left[\frac{\sin \Delta\gamma(x, y)}{\cos 2\Theta(x, y)} \right], \quad (5)$$

$$\Theta = \arctan \frac{U_x}{U_y}. \quad (6)$$

The performed analysis (Eqs. (1) to (6)) is devoted to the processes of formation of polarization-inhomogeneous images of optically thin (non-depolarizing) biological layers. That is why, these investigations can be efficient *in vitro* for histological sections of biological tissues with attenuation coefficient $\tau \leq 0.1$. In the case of real tissues (*in vivo* investigations), the above mentioned conditions are not met. Due to the multiple scattering process of forming the polarization structure of the object field is more complicated. The resulting polarization value (relation (3)) in each point of the field is generated both by the mechanisms of optical anisotropy (relations (1), (2), (4)-(6)) and subsequent cross-interference of the partial coherent waves. In this situation, there are three zones of diffraction [6] – boundary, Fresnel and Fraunhofer. In the first two zones of the polarization structure, the field varies in a continuous manner as the distance from the biological layer. In the far-field Fraunhofer diffraction zone, the object field (set of differently oriented plane-waves) is polarizationally stabilized. Therefore, this area is the most preferred for performing the medical research. However, due to the effects of space-frequency filtering the high frequencies, considerable information about the structure of the object is lost. In addition, large energy losses take place. The experimental way out of this situation can be optical realization of direct Fourier transform of the boundary field, which transforms it into a set of plane waves. In this case, we deal with formation of conditions inherent to the far diffraction zone, which provides minimization of the spatial frequency and energy losses. Based on this, we consider a model example (the situation of single scattering) forming the polarization structure of such field.

Taking into account the relations (2), the intensity, azimuth and ellipticity of polarization in each point of field in the Fourier plane can be determined from the following relations [21]

$$E_x(\mu, \nu) = \frac{A}{i\lambda f} \int_{-\infty}^{+\infty} U_x(x, y) \exp \left[-i \frac{2\pi}{\lambda f} (x\mu + y\nu) \right] dx dy, \quad (7)$$

$$E_y(\mu, \nu) = \frac{A}{i\lambda f} \int_{-\infty}^{+\infty} U_y(x, y) \exp \left[-i \frac{2\pi}{\lambda f} (x\mu + y\nu) \right] dx dy. \quad (8)$$

Here, E_x, E_y are amplitude distributions $U_x(\rho, \chi, \psi)$ and $U_y(\rho, \chi, \psi)$ in the focal plane with the spatial

frequencies $\nu = \frac{x}{\lambda f}$ and $\mu = \frac{y}{\lambda f}$, λ is the laser radiation wavelength; f – focal distance of polarization micro-objective.

By analogy with (4) to (6), the polarization maps ($\alpha^*(\mu, \nu)$, $\beta^*(\mu, \nu)$) of polarization inhomogeneous field in the Fourier plane are determined in accordance with the following relations

$$\alpha^*(\mu, \nu) = 0.5 \arcsin \left[\frac{\sin 2\Theta(\mu, \nu)}{\cos \chi(\mu, \nu)} \right]; \quad (9)$$

$$\beta^*(\mu, \nu) = 0.5 \arctan \left[\frac{\sin \chi(\mu, \nu)}{\cos 2\Theta(\mu, \nu)} \right], \quad (10)$$

where χ is the phase shift between the orthogonal component of laser field amplitude U_x , U_y in the Fourier plane, $\Theta = \arctan \frac{U_y}{U_x}$.

Due to the multiple scattering for objective (quantitative) estimation of distributions $\alpha^*(\mu, \nu)$ and $\beta^*(\mu, \nu)$, the statistic approach was used. Statistical moments of the first (Z_1), second (Z_2), third (Z_3) and fourth (Z_4) orders were calculated using the following algorithms

$$\begin{aligned} Z_1 &= \frac{1}{P} \sum_{j=1}^P (|q|)_j; Z_2 = \sqrt{\frac{1}{P} \sum_{j=1}^P ((q-Z_1)^2)_j}; \\ Z_3 &= \frac{1}{Z_2^3} \frac{1}{P} \sum_{j=1}^P ((q-Z_1)^3)_j; Z_4 = \frac{1}{Z_2^4} \frac{1}{P} \sum_{j=1}^P ((q-Z_1)^4)_j, \end{aligned} \quad (11)$$

where $P = 1280 \times 960$ – total amount of pixels of CCD-camera; $q \equiv (\alpha^*, \beta^*)$.

By means of Eq. (11), we have determined time stability of coordinate distributions $\alpha^*(\mu, \nu)$ and $\beta^*(\mu, \nu)$. Discrepancy between the statistical moments of the first (Z_1), second (Z_2), third (Z_3) and fourth (Z_4) orders for full measurement cycles did not exceed 4%.

3. Experimental results and discussion

There are two representative groups of patients with benign (adenoma – group 1 – 47 patients) and pre-cancer (keratoma – group 2 – 47 patients) skin changes were investigated.

Investigations were performed *in vivo* among the patients (30 males and 17 females) of age from 18 to 63 years in the region of neck, shoulder, arms and legs.

Fig. 1 represents an optical scheme of Fourier–Stokes polarimeter.

Illumination was performed with the beam of a He-Ne laser 1 ($\lambda = 0.6328 \mu\text{m}$, $G = 5.0 \text{ mW}$). The polarization illuminator consists of the input micro-objective 2, polarizer 3, quarter-wave plate 4, optical fiber 5, which provides formation of a laser beam with right circular polarization. The polarization micro-objective 7 (Nikon CFI Achromat P, focal distance – 30 mm, aperture – 0.1, magnification – 4 \times) is placed at the focal length from the skin surface 6. This scheme provides illumination of the human skin area ($S = 20 \text{ mm}^2$) and forms the Fourier spectrum of scattered radiation in the plane of CCD-camera 10 (The Imaging Source DMK 41AU02.AS, monochrome 1/2" CCD, Sony ICX205AL (progressive scan); resolution – 1280 \times 960; light sensitive area size – 7600 \times 6200 μm ; sensitivity – 0.05 lx; dynamic range – 8 bit; SNR – 9 bit). Besides, circular polarization of laser beam

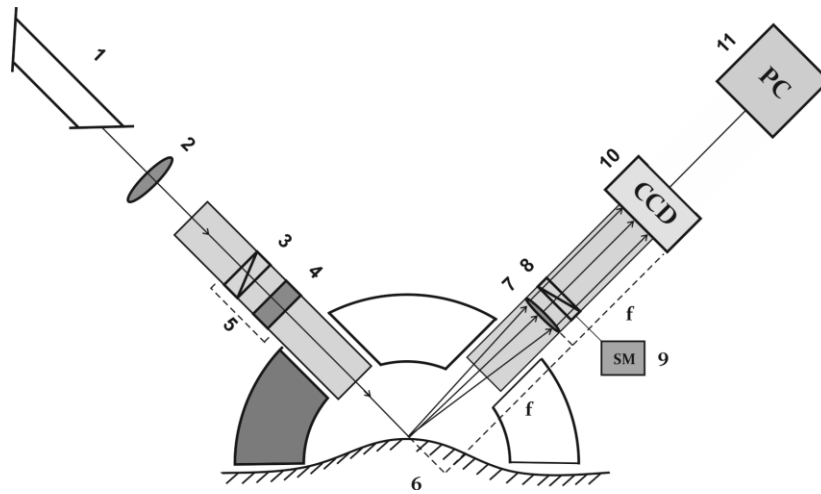


Fig. 1. Optical setup of Fourier–Stokes polarimeter: 1 – He-Ne laser, 2 – collimator; 3, 8 – polarizers; 4 – stationary quarter-wave plate; 5 – optical fiber; 6 – skin surface; 7 – polarization micro-objective; 9 – step motor, 10 – CCD camera; 11 – personal computer.

provides azimuthal invariance of the polarization inhomogeneous field in the Fourier plane.

The analysis of polarization structure inherent to the polarization inhomogeneous field in the Fourier plane is performed by means of polarizer-analyzer 8. By turning with the help of step motor 9 the analyzer axis at an angle Ψ within the range 0° to 180° , the arrays of minimal and maximal intensity levels $I_{\min}(m \times n)$, $I_{\max}(m \times n)$ were determined for every pixel $(m \times n)$ of CCD-camera, as well as for the rotation angles $\Psi(m \times n)(I(m \times n) \equiv \min)$ corresponding to them. The angular range of rotation was 5° ; duration of the entire measurement was 36 s. The coordinate structure of polarization-inhomogeneous speckle-field of the investigated skin areas remained stable. It was checked by cross-correlation comparison of the obtained images. The differences between the cross-correlation function of the field found for time periods of 2, 15 and 36 s didn't exceed 5%. Further, the coordinate distributions (polarization maps) of polarization azimuths and ellipticities of the field corresponding to reflected radiation were calculated using the following relations [20]

$$\alpha^*(m \times n) = \Psi(I \equiv \min) - \frac{\pi}{2},$$

$$\beta^*(m \times n) = \arctg\left(\frac{I_{\min}}{I_{\max}}\right). \quad (12)$$

By means of Eq. (11), we have determined the temporal stability of coordinate distributions $\alpha^*(\mu, \nu)$ and $\beta^*(\mu, \nu)$. Discrepancy between the statistical moments of the first (Z_1), second (Z_2), third (Z_3) and fourth (Z_4) orders for full measurement cycles did not exceed 4%.

Figs. 2 and 3 represent the polarization maps of azimuths $\alpha^*(\mu, \nu)$ (Figs. 2a, 2b), and ellipticities $\beta^*(\mu, \nu)$ (Figs. 3a, 3b) and the corresponding histograms of their values (Figs. 2c, 2d and 3c, 3d) of the Fourier spectra of reflected radiation by one patient's skin of the group 1 (b, d) and group 2 (a, c).

The obtained data show that:

1. Fourier spectra of laser radiation reflected by skin are polarization-inhomogeneous (Figs. 2a, 3b and 3a, 3b).
2. Histograms of values of azimuths and ellipticities of polarization inhomogeneous field in the Fourier plane are characterized by the maximal possible range ($\alpha = -90^\circ \dots 90^\circ$ and $\beta = -45^\circ \dots 45^\circ$) (Figs. 2c, 2d and 3c, 3d).

The obtained experimental results confirm the influence of optical anisotropy of human skin, as it has been predicted in the model (equations (1)-(10)), on formation of the polarization structure of polarization inhomogeneous field in the Fourier plane. It has been revealed that, depending on the pathology type (benign-malignant states) of skin, the polarization structure of polarization inhomogeneous field in the Fourier plane is different. In the case of keratoma (group 2), the dispersion of polarization parameters values for reflected radiation is less than for adenoma (group 1) (Figs. 2d and 3d). This fact, in our opinion, can be related with the destructive changes of birefringent structures of human skin [2, 7, 9, 11, 16].

It should be noted that the analyzed dependences (Fig. 2 and Fig. 3) are typical for other patients of both group. To obtain data of intergroup analysis, we have used methodology of differential diagnostics of skin pathology *in vivo* includes the following steps [22-24]:

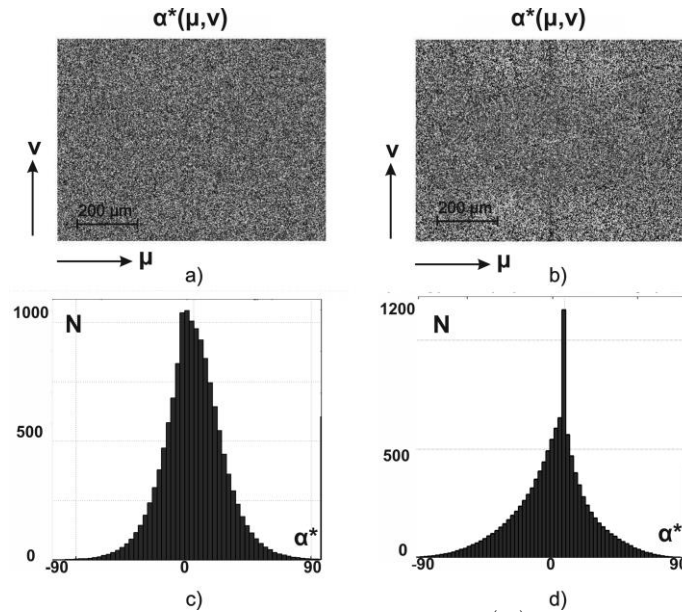


Fig. 2. Polarization maps $\alpha^*(\mu, \nu)$ (a, b) and the histograms of distributions $N(\alpha^*)$ (c, d) for laser images of histological sections taken from adenoma (a, c) and keratoma (b, d) of human skin.

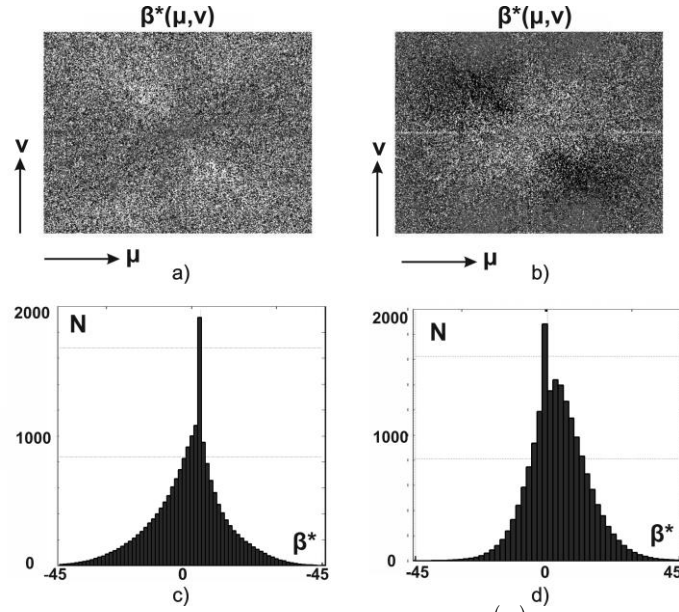


Fig. 3. Polarization maps $\beta^*(\mu, \nu)$ (a, b) and the histograms of distributions $N(\beta^*)$ (c, d) for laser images of histological sections taken from adenoma (a, c) and keratoma (b, d) of human skin.

3.1. Statistical analysis of polarization-inhomogeneous Fourier spectra of the object field of human skin

Methodology of differential diagnostics of skin pathology *in vivo* includes the following steps [22-24]:

1. Formation of representative samples of patient groups. For this purpose:
 - for each patient from the group 1 and group 2, we measured the distributions of values of polarization parameters (Eq. (11), Fig. 2 and Fig. 3) of Fourier spectra for reflected laser radiation;
 - for each distribution of values of $\alpha^*(\mu, \nu)$ and $\beta^*(\mu, \nu)$, we calculated the statistical moments of the 1st to 4th orders $R_{i=1;2;3;4}(\alpha^*)$ and $R_{i=1;2;3;4}(\beta^*)$ (Eq. (12));
 - for a specified significance level ($p = 0.05$), we calculated the statistical power by using the Z-test (Fisher's Z-criterion);
 - above mentioned steps were in progress for

statistical moments $\bar{R}_i(\alpha^*)$ and $R_i(\beta^*)$, until the range of statistical power reached 95%;

- as a result, we have obtained the statistically reliable number of patients within the groups 1 and 2 $n = 47$.
2. Differentiation between the group 1 and group 2 was reached using the following methodology:
 - within each set of values of statistical moments $R_{i=1;2;3;4}(q)$, we determined the average value $\bar{R}_{i=1;2;3;4}(q)$ and standard deviation $\sigma_{i=1;2;3;4}(q)$;
 - differences between the statistical sets $R_{i=1;2;3;4}(q)$ were significant in the case when the average value $\bar{R}_{i=1;2;3;4}(q)$ within the group 1 didn't "overlap" with the standard deviation $\sigma_{i=1;2;3;4}(q)$ within the group 2 and *vice versa* (see Table 1).
 3. For the possible clinical application of this method, we used the traditional for probative medicine operational characteristics: sensitivity

Table 1. Statistical moments of the 1st to 4th orders for the distributions of polarization azimuths ($\alpha^*(\mu, \nu)$) and ellipticities ($\beta^*(\mu, \nu)$) of human skin Fourier spectra.

Parameters	$\alpha^*(\mu, \nu)$		$\beta^*(\mu, \nu)$	
	Group 1	Group 2	Group 1	Group 2
	$R_i \pm \sigma_i$		$R_i \pm \sigma_i$	
R_1	0.15±0.008	0.10±0.007	0.07±0.005	0.05±0.004
R_2	0.35±0.025	0.22±0.017	0.15±0.009	0.09±0.007
R_3	1.89±0.12	0.75±0.13	0.5±0.032	0.82±0.061
R_4	1.88±0.11	2.76±0.16	0.83±0.057	1.34±0.09

each of the obtained eight sets of values of

$\left(Se = \frac{a}{a+b} 100\% \right)$, specificity $\left(Sp = \frac{c}{c+d} 100\% \right)$ and balanced accuracy $\left(Ac = \frac{Se+Sp}{2} \right)$, where a and b are the number of correct and wrong diagnoses within the group 2; c and d – the same within the group 1. For this purpose:

- within both groups of patients for the distributions of values of each statistical moments $R_{i=1;2;3;4}(q)$, we chose cutoff of 3σ (99.72% of all possible values of changes of R_i);
- sequentially, we determined the number of “false negative” (b) and “false positive” (d) conclusions;
- for each of statistical moments $R_{i=1;2;3;4}(q)$, we calculated the values of sensitivity Se , specificity Sp and balanced accuracy Ac of diagnostical test of Fourier polarimetry for laser radiation reflected by human skin (see Table 2);
- from the obtained data [$Se(R_i(q))$, $Sp(R_i(q))$, and $Ac(R_i(q))$], we chose the maximal values of operational characteristics (highlighted by grey color in Table 2).

Therefore, operational characteristics of the method of Fourier polarimetry of reflected by skin laser radiation in the tasks of differentiation of benign and malignant states reached the excellent quality of diagnostic test – $Ac(\alpha^*, \beta^*) = 92...96\%$ [22].

4. Conclusions

1. The distributions of polarization parameters of radiation reflected by skin (adenoma, keratoma) in the Fourier plane have been determined.
2. The set of statistical (statistical moments of the 1st to 4th orders) parameters characterizing the distributions of azimuths and ellipticities of polarization inhomogeneous field in the Fourier plane have been determined. They appear to be sensitive for diagnostics and differentiations of pathological anisotropy changes of human skin.
3. The operational characteristics of the Fourier polarimetry method for laser radiation reflected by human skin have been determined. The excellent quality of diagnostic tests based on this optical method in the task of differentiation of benign and malignant states has been achieved.

Table 2. Operational characteristics of the method of Fourier polarimetry of laser radiation reflected by skin.

Parameters, %	$\alpha^*(\mu, \nu)$			$\beta^*(\mu, \nu)$		
<i>Se</i>	R_1	61	$a = 29, b = 18$	R_1	58	$a = 27, b = 20$
	R_2	72	$a = 33, b = 14$	R_2	65	$a = 31, b = 16$
	R_3	95	$a = 45, b = 2$	R_3	88	$a = 41, b = 6$
	R_4	86	$a = 42, b = 5$	R_4	93	$a = 43, b = 4$
<i>Sp</i>	R_1	66	$c = 32, d = 15$	R_1	64	$c = 30, d = 17$
	R_2	75	$c = 35, d = 12$	R_2	73	$c = 33, d = 14$
	R_3	95	$c = 44, d = 3$	R_3	82	$c = 38, d = 9$
	R_4	88	$c = 41, d = 6$	R_4	88	$c = 40, d = 7$
<i>Ac</i>	R_1	64	$a = 29, b = 18$ $c = 22, d = 15$	R_1	63	$a = 27, b = 20$ $c = 30, d = 17$
	R_2	73	$a = 33, b = 14$ $c = 35, d = 12$	R_2	67	$a = 31, b = 16$ $c = 33, d = 14$
	R_3	96	$a = 42, b = 5$ $c = 44, d = 3$	R_3	85	$a = 41, b = 6$ $c = 38, d = 9$
	R_4	87	$a = 42, b = 5$ $c = 41, d = 6$	R_4	90	$a = 43, b = 4$ $c = 40, d = 7$

References

1. Preuss L.E. and Profio A.E. Optical properties of mammalian tissue: Introduction by the feature editors. *Appl. Opt.* 1989. **28**. P. 2207–2207.
2. Cheong W.-F., Prahl S.A., Welch A.J. A review of the optical properties of biological tissues. *IEEE J. Quantum Electron.* 1990. **26**. P. 2166–2185.
3. Prahl S.A., Keijzer M., Jacques S.L., Welch A.J. A Monte Carlo model of light propagation in tissue. *Proc. SPIE.* 1989. **IS 5**. P. 102–111.
4. Polyanskii V.K., Angelsky O.V., Polyanskii P.V. Scattering induced spectral changes as a singular optical effect. *Optica Applicata.* 2002. **32**. P. 843–848.
5. Brusciaglioni P., Zaccanti G., and Wei Q. Transmission of a pulsed polarized light beam through thick turbid media: Numerical results. *Appl. Opt.* 1993. **32**. P. 6142–6150.
6. Angelsky O.V., Tomka Yu.Ya., Ushenko A.G., Ushenko Y.G., Yermolenko S.B. 2-D tomography of biotissue images in pre-clinic diagnostics of their pre-cancer states. *Proc. SPIE.* 2005. **5972**. P. 158–162.
7. Pierce M.C., Strasswimmer J., Park B. Hyle, Cense B., de Boer J.F. Birefringence measurements in human skin using polarization-sensitive optical coherence tomography. *J. Biomed. Opt.* 2004. **9**. P. 287–291.
8. de Boer J.F., Milner T.E., van Gemert M.J.C., and Nelson J.S. Two-dimensional birefringence imaging in biological tissue by polarization-sensitive optical coherence tomography. *Opt. Lett.* 1997. **22**. P. 934–936.
9. Saxer C.E., de Boer J.F., Park B.H., Zhao Y., Chen Z., Nelson J.S. High-speed fiber based polarization-sensitive optical coherence tomography of in vivo human skin. *Opt. Lett.* 2000. **25**. P. 1355–1357.
10. Ushenko A.G. Polarization correlometry of angular structure in the microrelief pattern of rough surfaces. *Optics and Spectroscopy.* 2002. **92**. P. 227–229.
11. de Boer J.F., Milner T.E. Review of polarization sensitive optical coherence tomography and Stokes vector determination. *Biomed. Opt.* 2002. **7**. P. 359–371.
12. Yasuno Y., Makita S., Sutoh Y., Itoh M., Yatagai T. Birefringence imaging of human skin by polarization-sensitive spectral interferometric optical coherence tomography. *Opt. Lett.* 2002. **27**. P. 1803–1805.
13. Ushenko Yu.A., Boychuk T.M., Bachynsky V.T., Mincer O.P. Diagnostics of structure and physiological state of birefringent biological tissues: Statistical, correlation and topological approaches, in: *Handbook of Coherent-Domain Optical Methods*. Springer Science+Business Media, New York, 2013. P. 107–148.
14. Angelsky O.V., Zenkova C.Y., Gorsky M.P., Gorodynśka N.V. Feasibility of estimating the degree of coherence of waves at the near field. *Appl. Opt.* 2009. **48**, No. 15. P. 2784–2788.
15. Angelsky O.V., Besaha R.N., Mokhun A.I., Mokhun I.I., Sopin M.O., Soskin M.S., Vasnetsov M.V. Singularities in vectorial fields. *Proc. SPIE.* 1999. **3904**. P. 40.
16. Angelsky O.V., Bekshaev A.Ya., Maksimyak P.P., Maksimyak A.P., Hanson S.G., Zenkova C.Yu. Self-action of continuous laser radiation and Pearcey diffraction in a water suspension with light-absorbing particles. *Opt. Exp.* 2014. **22**, No. 3. P. 2267–2277.
17. Angelsky O.V., Bekshaev A.Ya., Maksimyak P.P., Maksimyak A.P., Hanson S.G. Measurement of small light absorption in microparticles by means of optically induced rotation. *Opt. Exp.* 2015. **23**, No. 6. P. 7152–7163.
18. Ushenko Yu.O., Tomka Yu.Ya., Telenga O.I., Misevitch I.Z., Istratiy V.V. Complex degree of mutual anisotropy of biological liquid crystals nets. *Opt. Eng.* 2011. **50**. P. 039001.
19. Karachevtsev A.O. Fourier Stokes-polarimetry of biological layers polycrystalline networks. *Semiconductor Physics, Quantum Electronics & Optoelectronics.* 2012. **15**, No. 3. P. 252–268.
20. Ushenko V.A., Sidor M.I., Marchuk Y.F., Pashkovskaya N.V., Andreichuk D.R. Azimuth-invariant Mueller-matrix differentiation of the optical anisotropy of biological tissues. *Optics and Spectroscopy.* 2014. **117**, No. 1. P. 152–157.
21. Ushenko V.A., Zabolotna N.I., Pavlov S.V., Burcovets D.M., Novakovska O.Yu. Mueller-matrices polarization selection of two-dimensional linear and circular birefringence images. *Proc. SPIE.* 2013. **9066**, Eleventh International Conference on Correlation Optics. P. 90661X.
22. Ushenko V.A., Gorsky M.P. Complex degree of mutual anisotropy of linear birefringence and optical activity of biological tissues in diagnostics of prostate cancer. *Optics and Spectroscopy.* 2013. **115**, No. 2. P. 290–297.
23. Ushenko Yu.A., Gorsky M.P., Dubolazov A.V., Motrich A.V., Ushenko V.A., Sidor M.I. Spatial-frequency Fourier polarimetry of the complex degree of mutual anisotropy of linear and circular birefringence in the diagnostics of oncological changes in morphological structure of biological tissues. *Quantum Electronics.* 2012. **42**, No. 8. P. 727.
24. Ushenko V.A. Complex degree of mutual coherence of biological liquids, in: *ROMOPTO International Conference on Micro- to Nano-Photonics III* (P. 88820V–88820V), International Society for Optics and Photonics, 2013.
25. Ushenko Yu.O., Dubolazov O.V., Karachevtsev A.O., Gorsky M.P., Marchuk Y.F. Wavelet analysis of Fourier polarized images of the human bile. *Appl. Opt.* 2012. **51**, No. 10. P. C133–C139.

26. Ushenko Yu.A., Ushenko V.A., Dubolazov A.V., Balanetskaya V.O., Zabolotna N.I. Mueller-matrix diagnostics of optical properties of polycrystalline networks of human blood plasma. *Optics and Spectroscopy*, 2012. **112**, No. 6. P. 884–892.
27. Ushenko Yu.A., Tomka Yu.Ya., Dubolazov A.V. Laser diagnostics of anisotropy in birefringent networks of biological tissues in different physiological conditions. *Quantum Electronics*. 2011. **41**, No. 2. P. 170–175.
28. Ushenko Yu.A., Dubolazov A.V., Balanetskaya V.O., Karachevtsev A.O., Ushenko V.A. Wavelet-analysis of polarization maps of human blood plasma. *Optics and Spectroscopy*. 2012. **113**, No. 3. P. 332–343.
29. Goodman J.W. Statistical properties of laser speckle patters. In: *Laser Speckle and Related Phenomena*, Ed. J.C. Dainty. Berlin, Springer-Verlag, 1975. P. 9–75.
30. Cassidy L.D. Basic concepts of statistical analysis for surgical research. *J. Surgical Res.* 2005. **128**. P. 199–206.
31. C.S. Davis, *Statistical Methods of the Analysis of Repeated Measurements*. New York, Springer-Verlag, 2002.
32. A. Petrie, B. Sabin, *Medical Statistics at a Glance*. Blackwell Publishing, 2005.

RETRACTED